Engineering Structures 304 (2024) 117605

Contents lists available at ScienceDirect

Engineering Structures

journal homepage: www.elsevier.com/locate/engstruct

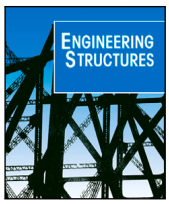

Shape and loading imperfection sensitivity of the vibration-correlation technique for buckling analysis of cylindrical shells

T.D. Baciu [a,b,*], F. Franzoni [a], R. Degenhardt [a,b,c], K. Kalnins [d], C. Bisagni [e]

[a] DLR German Aerospace Center, Germany
[b] University of Bremen, Germany
[c] Private University of Applied Sciences Göttingen, Germany
[d] Riga Technical University, Latvia
[e] Politecnico di Milano, Italy

ARTICLE INFO

Keywords:
Vibration correlation technique
Shell buckling
Imperfection sensitivity

ABSTRACT

A numerical investigation was performed to assess the feasibility of the Vibration Correlation Technique (VCT) to predict the buckling load of cylindrical shells under compression, taking into account shape and loading imperfections. The capability of VCT to provide reliable buckling load predictions using load steps before and after local buckling occurred was also assessed, employing two different VCT procedures and buckling analyses. It was found that the buckling load predictions using VCT are generally insensitive to shape and loading imperfections, but that certain shape imperfections might give unconservative predictions, behaviour which generally can be identified with ease. Increasing the imperfection amplitudes increased the number of secondary buckling events, which in turn decreased the robustness of the VCT to predict the global buckling load when load steps before local buckling occurred were used. Based on numerical results, predicting the global buckling load using load steps after local buckling occurred seemed feasible, but might provide unconservative results. In this case, using a novel empirical VCT procedure and taking into account shape imperfections in the buckling analysis significantly increased the reliability of the VCT predictions. The more conservative outcome of the empirical VCT procedure and the robustness of VCT predictions using load steps after local buckling occurs was also shown to hold true when using experimental data from two cylinders subjected to axial compression.

1. Introduction

Research on cylindrical shell buckling represents an extensive topic with a long history, which remains highly active to this day due to the large use of these types of structures in the aerospace, marine, or energy sectors, among others. Additionally, their high sensitivity to imperfections also represents a key driver to the ongoing interest in this field. For cylindrical shells, buckling under axial compression is particularly sensitive to imperfections, as in their presence the load carrying capacity of these structures can be reduced significantly. The NASA SP-8007 [1] guideline on buckling of thin-walled circular cylinders recommends empirical knockdown factors within the 0.18–0.84 interval ($r/t < 1500$), as a function of the ratio between the radius and the thickness of the cylinders. However, these empirical lower bounds are often found to be over-conservative, thus lowering the structural efficiency of an article in service [2–4].

Out-of-plane (OoP) imperfections are of paramount importance in improving the accuracy of the predicted buckling load for cylindrical shells under axial compression, aspect observed as early as 1914 by Southwell [5]. Next to these, loading, thickness, boundary conditions, or material imperfections can also significantly lower the buckling load of these structures [2,6,7].

Finite element (FE) analysis is a powerful tool that can be used to significantly improve the efficiency of shell structures. Nowadays FE tools are used to study complex structural behaviours, the correlation between FE results and experimental data being generally very good, provided that the model is built with sufficient level of detail. The high confidence in FE analyses resulted in an extensive use of this tool in designing and sizing load bearing structures across multiple industries, enabling a better design optimisation, at a faster rate, and reducing the need of costly experimental campaigns [8,9]. For buckling of cylindrical shells in particular, it enabled extensive studies on the influence of multiple factors over their structural response. Aspects like the influence of imperfections such as shape, loading, thickness and boundary conditions over the behaviour, or the vibration response, of

* Corresponding author at: DLR German Aerospace Center, Germany.
E-mail address: theodor.baciu@dlr.de (T.D. Baciu).

https://doi.org/10.1016/j.engstruct.2024.117605
Received 28 August 2023; Received in revised form 11 December 2023; Accepted 30 January 2024

a structure can all be accurately represented by FE models and further investigated, the numerical results being successfully validated through experiments [3,10–18].

Regardless of the design approach, structural elements often need to be experimentally tested and the measured data must be correlated with the analytical/numerical data to validate their design. While imperfections types such as shape and thickness can be accurately measured and implemented in numerical analyses, loading, boundary conditions and material imperfections are more difficult to include in the analysis prior testing, thus representing a possible source of a poor correlation. Non-destructive methods are one viable solution in determining the buckling loads for cylindrical shells under compression, as they inherently capture all the particularities of the item tested, including its test set up. One such method is the vibration-correlation technique (VCT), which can also be used to determine the in-situ test boundary conditions [19], or the fiber volume fraction of composite structures [20]. When used to determine the buckling load of a structure, the change in the structure's vibration response with the applied load is used to extrapolate the buckling load from measurements taken at lower load levels.

Performing VCT to predict the buckling load of a structure is a fairly old concept, with some of the earliest descriptions and experimental validations of the relation between a structure's vibration response and its loading being reported at the beginning of the 20th century [21,22]. In this early VCT formulation for perfect, simply supported, beams and for the vibration mode identical with the buckling mode, the relation between the applied load P and the frequency F of a vibration mode k (F_k) was defined as follows:

$$f_k^2 + p = 1 \tag{1}$$

where p is the ratio between the applied load P and the critical buckling load P_{cr} and f_k is the ratio between the vibration mode frequency under load F_k and its unloaded counterpart $F_{0,k}$. Furthermore, other boundary conditions showed little variation from this linear relationship, making this VCT approach more feasible for practical testing conditions [23]. This relation could then be used to extrapolate the value P at which the square of the frequency ratio f_k^2 becomes 0. In this VCT approach, as well as for other VCT approaches, the only non-empirical quantity is P_{cr}. While the means by which this value is obtained (analytical, semi-analytical, numerical) and its influence over the robustness of the VCT prediction has not yet been studied, the most common approach is to obtain this value by numerical means.

After these initial investigations at the beginning of the 20th century, the level of interest in further investigating and exploiting the relation between a structure's vibration response and its loading slowly picked up, focusing initially on beam structures, for which buckling loads and boundary conditions were estimated [23–28]. Further investigations since the 30s on columns [29–31] and since the 40s on circular plates [32,33] found that this linear relationship does not hold true in presence of imperfections, shape in particular, with significant deviations from linearity being observed as the load approached the buckling load. Other compression members like trusses and frames were shown in a study around the middle of the 20th century to display a similar behaviour [34,35]. Nevertheless, the linear relationship for perfect simply supported columns and polygonal plates was analytically validated in [31–34,36]. Similarly, while an analogous linear relationship as the one shown in (1) was analytically verified for simply supported cylindrical shells under external pressure or axial compression [37], aspect also experimentally found for the axial compression case [38], this behaviour was also not found to hold true in presence of imperfections [39–43]

Following the consistently found deviation from linearity in the relation between the squared frequency and applied load ratios, a novel VCT procedure was proposed for columns and shells, where the buckling load is found using the following relation:

$$(1-p)^2 + (1-\xi_k^2)(1-f_k^4) = 1 \tag{2}$$

by extrapolating the value of $(1\text{-}p)^2 = \xi_k^2$ at $(1\text{-}f_k^4) = 1$, where ξ_k^2 represents the load drop due to imperfections and must be positive for it to have a physical meaning.

However, the above VCT method was found by Arbelo et al. [19] to be unreliable for unstiffened composite cylindrical shells, as often the value of ξ_k^2 was negative. In this publication the authors also proposed a new approach, analytically verified in [44], in which the following quadratic relation was found between $(1\text{-}p)^2$ and $(1\text{-}f_k^2)$:

$$(1-p)^2 = [1-(1-f_k^2)]^2 \tag{3}$$

In this approach the buckling load is found using the following equation:

$$P_{VCT,k} = P_{cr}\left(1-\sqrt{\xi_k^2}\right) \tag{4}$$

where ξ_k^2 represents the minimum value of the quadratic equation best fitted to the points of the $(1\text{-}p)^2$ vs $(1\text{-}f_k^2)$ VCT characteristic chart. This recent development boosted the interest in VCT, with multiple experimental campaigns validating the aforementioned approach being published afterwards [17,19,44–57]. Furthermore, recent developments in reusable space structures represent an additional important driver for further research on VCT, which can serve as a reliable tool to assess their potential loss of load carrying capabilities upon reuse. This increased interest led to yet another relation between the load applied and the structure's frequency response being proposed in [55], where $(1\text{-}p)^2$ is plotted against (1-f), the rest of the procedure being identical to the one previously described. This novel procedure is referred to here as the empirical VCT method, due to the lack of an analytical validation. The authors investigated the robustness of both the Arbelo's procedure and the proposed empirical one for multiple nominally identical cylindrical shells of an identical layup, using two load introduction methods (parallel plates and hemispherical joints) and two different end supports (steel rings and potting resin). It was reported that the empirical method tends to be slightly more conservative and with a lower variation, both methods appearing relatively insensitive towards the cylinder geometry, imperfection, end supports, or load introduction procedure. Nevertheless, there were a few cases in which VCT failed to provide a robust buckling load prediction, most likely owing to a particularity related to either its imperfection, and/or its testing method.

Besides the focus on validating this non-destructive method for multiple types of structures and loading environments, focus was also given to increase the efficiency of its numerical implementation, achieved primarily through a more efficient eigenvalue analysis [17,58,59]. In [59] the eigenvalue analyses were performed concurrently for various ratios of P_{cr} and the buckling loads were estimated via VCT for axial compression and axial compression combined with internal pressure, or torque. The agreement between the VCT buckling load estimation and the experimental buckling load under axial compression, or the buckling load obtained via explicit dynamic analyses under combined compression with internal pressure/torque, was excellent, the computational time being one order of magnitude lower when compared to explicit dynamic and Riks analysis procedures. In [58] and [17] reduced order models (based on a proper orthogonal decomposition and a combined approximation method respectively) were built using the frequency response in the unloaded and relatively highly loaded states from full order models. Then, these reduced order models were used to perform the required frequency eigenvalue analyses, at a higher computational efficiency, needed to perform VCT. The buckling load estimations based on these approaches were also in a very good agreement with the experimental and explicit dynamic analyses results, again the computational time being an order of magnitude lower with respect to the explicit dynamic numerical procedure.

While the relatively large number of experimental campaigns where the buckling load predictions using VCT were reliable, therefore, also the large number of imperfection patterns inherent to those structures,

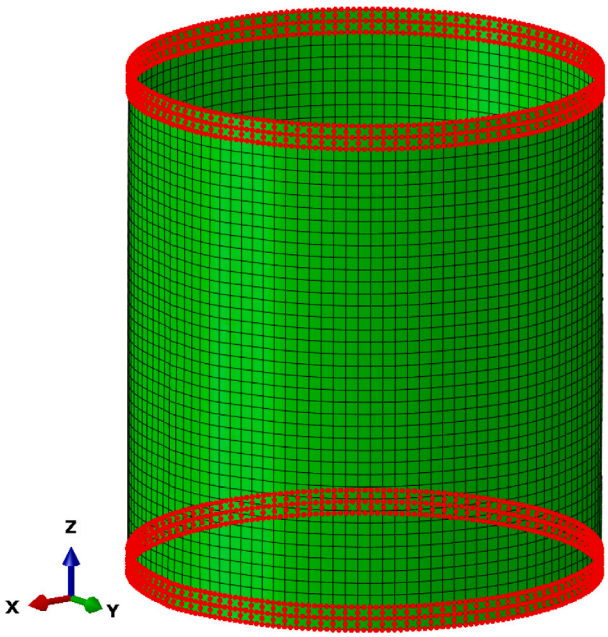

Fig. 1. SST1 cylinder FE model.

suggests that VCT seems to be fairly insensitive to various types of imperfections, to the author's best knowledge, studies focusing on the sensitivity of this non-destructive method to shape and loading imperfections have not yet been published.

In this paper, the influence of shape and loading imperfections on the feasibility of VCT for predicting the buckling load of cylindrical shells under axial compression is numerically studied, employing established numerical procedures validated by experimental data. Representative shape and loading imperfections were applied to a cylindrical shell in various magnitudes and the reliability of VCT to predict the buckling loads obtained via non-linear FE analyses was studied. Furthermore, the importance of including shape imperfections in the buckling analysis to determine the value of P_{cr} used in the VCT predictions was also assessed, together with Arbelo's and the novel empirical VCT procedures. Then, the experimental results from the VCT experimental tests of two different cylinders are used to successfully verify the observations drawn from the numerical investigation.

2. Methodology

The geometry used to build the FE model for the numerical analyses is the one of the SST1 cylinder, for which VCT provided a robust buckling load prediction, as reported in [51]. This particular cylinder was used due to its high imperfection sensitivity, having a knockdown factor of approximately 0.38 (0.32 according to the NASA SP 8007), and reliable VCT predictions for multiple load ratios.

The AISI 304 steel cylinder was manufactured by laser welding a single plate rolled up to the desired curvature. The uniform load introduction was ensured by clamping the top and bottom edges in potting resin, together with metallic support rings placed at the inner side of the edges, and further gluing its edges to the load introduction plates with epoxy. Furthermore, a hemispherical joint was also placed between the machine's cross-head and the loading plate, thus allowing self-alignment, reducing the bending effects and minimising loading imperfections [51]. Table 1 provides a summary of the geometry, material properties, plus the critical, experimental and VCT predicted buckling loads of the SST1 cylinder, where the P_{cr} is based on a linear buckling analysis of the FE model.

Table 1
SST1 cylinder geometry, material properties and reference buckling loads.

ρ [g/cm^3]	7.8	L [mm]	500
μ_{12}	0.29	r [mm]	250
E [GPa]	193	t [mm]	0.5
G [GPa]	77	P_{cr} [kN]	183.3
S_Y [MPa]	215	P_{exp} [kN]	70.2
S_U [MPa]	505	P_{VCT} [kN]	70.22 at 81.5%P_{exp}

The FE model was built in Abaqus [60] and meshed with S8R elements, the mesh convergence analysis showing that 120 elements along the circumference and 42 along the axial direction (element aspect ratio $\approx$ 1) was sufficient to accurately model the cylinder's compression response. All degrees of freedom over the 25 mm areas in contact with the outer resin rings and inner steel support rings, except the axial translations, were restrained and the load was introduced through displacements applied on the top and bottom edge nodes. The FE model used can be seen in Fig. 1, where the top and bottom areas over which the boundary conditions were applied are highlighted.

The OoP imperfection, shown here in Fig. 2, was measured on the inner side of the cylinder and was implemented in the FE model using an inverse interpolation method to adjust the radial coordinates of the nodes, approach described in more detail in [3], this approach, or very similar ones, being validated in several experimental campaigns [14,19,46,57,61–63]. Multiple amplitudes of the original measurement magnitude, varying from 0.01 and up to 3 times the measured one, were introduced to study the influence of shape imperfections on the VCT buckling load prediction capabilities.

For the loading imperfection, measured edge in-plane (IP) patterns were used to model an uneven loading of the cylinder edges. Fig. 3 shows a schematic of the procedure to introduce the loading imperfections using the patterns published in the NASA SP 8007 [1] and shown in Fig. 4, using the top edge as an example. These measurements were normalised such that they laid between 0 and 1, the shown magnitudes being equivalent with displacements in mm imposed to the nodes of the cylinder edges to model the loading imperfection. Starting from the FE model built using the nominal cylinder geometry, where the top edge is perfectly flat, as shown in Fig. 3(a), the node coordinates along the Z axis of the top edge were modified according to the measured top pattern, such that the cylinder was extended. Fig. 3(b) shows a schematic of the top edge nodes at the end of this process, where dz1 represents the amount by which the z coordinate of node 1 was modified. Then, in an initial non-linear step, axial displacements were applied to the edge nodes such that at the end of the step the edges were perfectly flat again, introducing thus an uneven loading. This procedure is shown here in Fig. 3(c), where now dz1 represents the magnitude of the axial displacement applied, of the same magnitude as the amount by which the z coordinate of that node was altered, and dz represents a small uniform displacement applied to all top edge nodes.

A similar procedure was used for the bottom edge nodes, the difference being that the nominal z nodal coordinates were decreased and brought back in the same non-linear step, without adding a uniform displacement. This procedure was done to simulate the way the top and bottom edges flatten as the load introduced by the top loading plate increases. Similar approaches were also used in multiple studies [15,64–68], where the influence of loading imperfections and uneven settlement on the buckling response of shells was investigated.

After the load imperfection was introduced, a uniform displacement was further applied on the top edge nodes in a second non-linear step. Similar as for the OoP imperfection, multiple IP imperfection amplitudes were used, ranging from 0.01 to 0.25, where these amplitudes represent the maximum displacement in mm applied as a loading imperfection.

Shape and loading imperfections are known as possible triggers of local buckling [15,63,67,69]. This aspect was also found here and was characterised by a change in the load–displacement response,

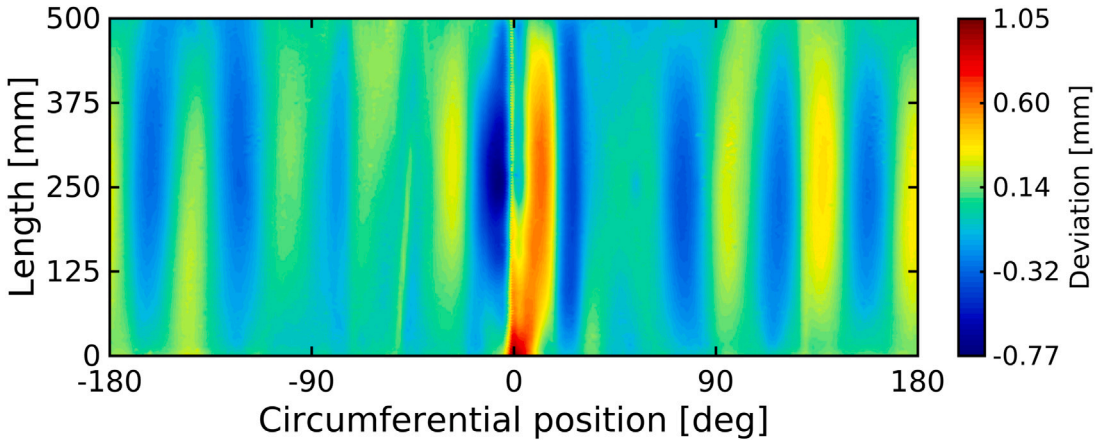

Fig. 2. SST1 OoP imperfection pattern measured on the inner surface of the cylinder [51].

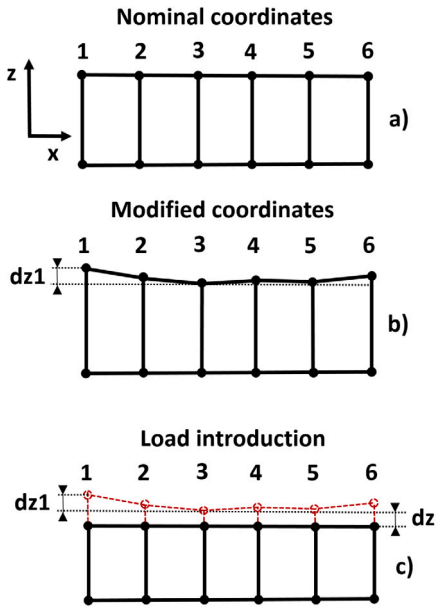

Fig. 3. Load imperfection introduction.

associated with either the apparition of a localised pattern, or in the case of multiple such events occurring, by a change in the localised buckling pattern. The occurrence of local buckling implied that, instead of single and approximately linear relation between the applied displacement and reaction load observed on the load–displacement curves up to the global buckling point, multiple such quasi-linear regions were observed. These regions are identified in the load–displacement curves as the regions in which there is a roughly linear load–displacement response and at the end of which a decrease in the load carried by the structure was found. In these regions the apparent stiffness, the ratio between the change in load and the one in displacement, tends to slowly drop with increasing the load level (quasi-linear response), becoming negative when the load carried by the structure decreases while the displacement increases. These load-drops in the load–displacement curves were associated with either local, or global, buckling and the quasi-linear regions prior these load-drops are here referred to as VCT regions.

The change in the shell's equilibrium state as a result of local buckling occurring could also cause a significant change in its frequency response, meaning that a VCT buckling load prediction using load steps defined both before and after such events could be meaningless. Therefore, when such events occurred, VCT load steps were explicitly defined between such events to perform a sensitivity study involving the use of different quasi-linear regions, values of P_{cr} and VCT procedures. The procedure used to define the VCT load steps is shown in Fig. 5.

Once the non-linear analysis was completed, a script looping through the load–displacement response was used to define the VCT load steps for that specific analysis. At the beginning of the procedure, the non-linear global buckling load P_{nl} and its time increment number inc_{max} were fed as inputs, the former being used in the VCT load step definition criteria, while the latter was used to break the loop. Furthermore, the number of VCT regions within the analysis was initialised with one and its corresponding starting load F_{start} with zero. The initial stiffness S_{ini} used in the VCT load steps definition criteria was also defined at this stage, based on the first two increments, and the loop was started from the second increment ($i = 1$). Then, the increment number was increased until a load drop was detected, or the maximum increment number was reached, point at which the maximum load in that region F_{end} was retrieved and the first VCT load step definition criterion was applied. This initial criterion consisted in checking if the difference between the minimum and maximum load of the region is larger than 10% of the global non-linear buckling load P_{nl}. While mostly irrelevant when defining VCT load steps in the initial VCT region, this criterion was needed to avoid defining a large number of irrelevant load steps when multiple load drops were found within a negligible load ratio difference. This behaviour was generally seen either immediately after local buckling occurred, or at load levels close to the global buckling load. If this first criterion was satisfied, the average apparent stiffness in that region S_{start_end} was also computed based on the load and displacement values between consecutive time increments within the entire region and used in the second VCT load step definition criterion. This second criterion comprised in checking whether the average stiffness in that region was larger than half of the initial stiffness. While also mostly irrelevant when defining VCT load steps in the initial region, this criterion was useful to avoid defining load steps where the compressive response of the model was highly non-linear due to significant bending effects. These regions typically occurred after multiple changes in the localised buckling patterns and at relatively high load ratios, exhibiting a severe and constant decrease in the apparent stiffness and at a negligible change in the additional load carried. If this criterion was also satisfied, the VCT load steps were defined and the VCT region number was updated. Then, the loop was stopped if the increment was the one at which P_{nl} was found and if not, the increment number was further increased until an increase in the load carried was observed, point at which the minimum load level of the VCT region F_{start} was updated. Here F_{start} was updated including a tolerance F_{tol}, instead of simply using F_{i-1}, to avoid defining a VCT

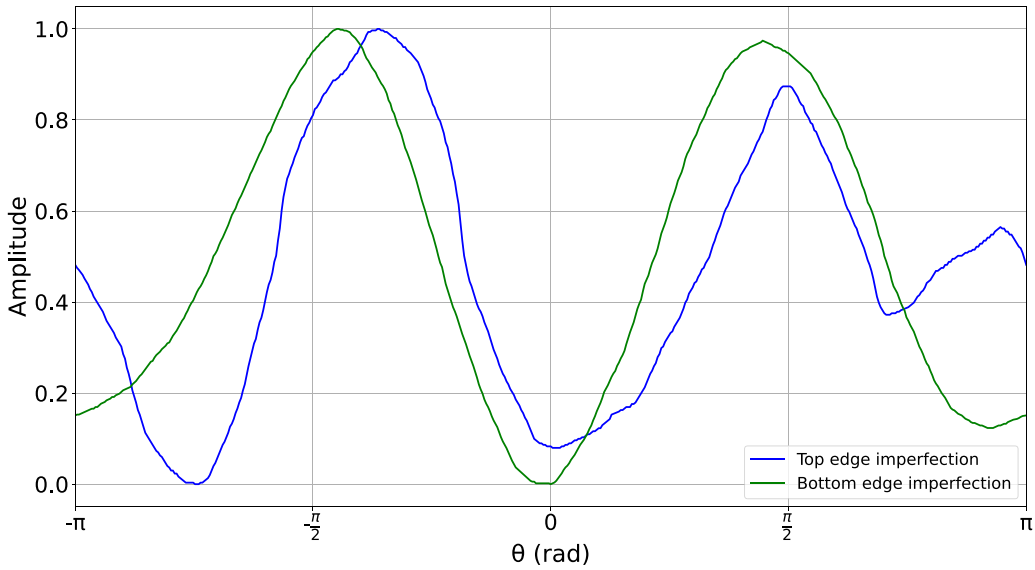

Fig. 4. IP imperfection patterns of the top and bottom edges [1].

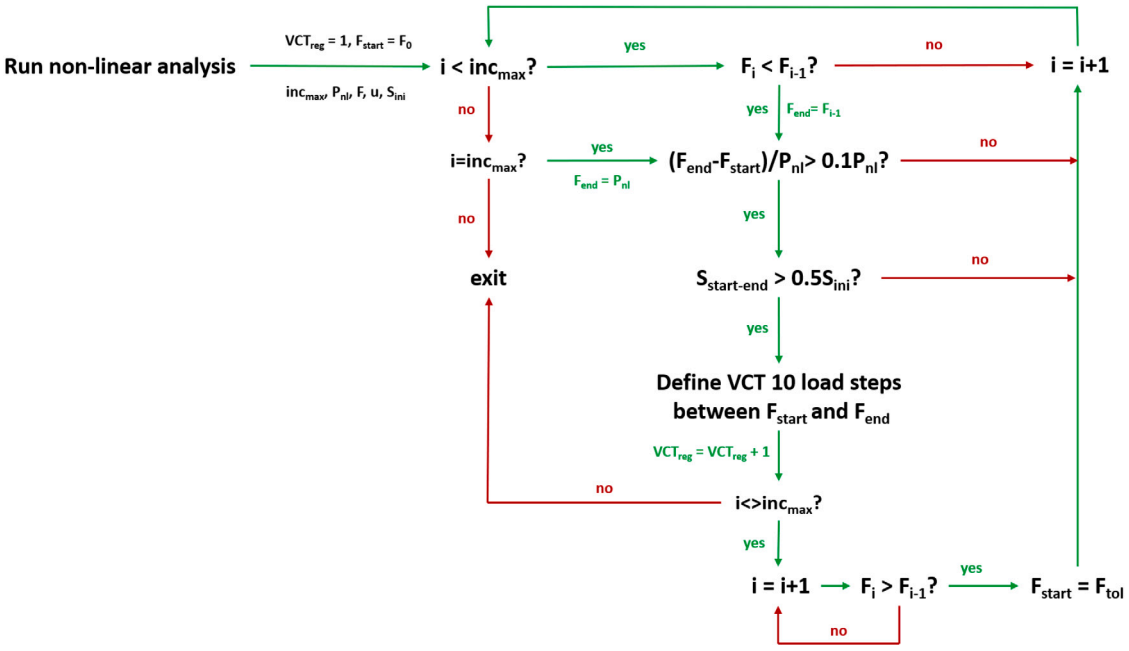

Fig. 5. VCT load steps definition procedure.

load step in the potentially highly non-linear region immediately after an increase in the load carried was observed. The definition of F_{tol} was displacement based and it was taken as the load corresponding to $1.01u_{i-1}$, this value being sufficient in successfully avoiding the aforementioned highly non-linear regions. After F_{start} was updated, the entire process was repeated until the maximum increment of interest inc_{max} was reached, at which the VCT load step definition procedure was completed.

In the VCT regions beyond the initial one, the vibration mode frequency in unloaded state $F_{0,k}$ was no longer applicable given the general lack of continuity of the vibration modes across the VCT regions and the vibration mode frequency of the first load step in that specific VCT region was instead used as a reference. Moreover, when multiple VCT regions were found, an investigation on whether the VCT is more likely to predict the local, or the global buckling load, was also performed. In addition, two sets of P_{cr} values, with and without the OoP imperfections introduced, were used to identify which one would be best suited to use for robust VCT buckling load predictions. Lastly, the novel VCT empirical procedure in which $(1\text{-}p)^2$ is plotted against (1-f) was also compared against the established analytical relation proposed by Arbelo.

3. Results

3.1. Buckling

The critical buckling loads P_{cr} were obtained by performing linear buckling analyses, where the nodes in the areas overlapping with the resin rings and inner steel rings were coupled with reference points at the ends of the cylinder and on which the same boundary conditions as for the non-linear models were specified. Then, the axial load was introduced by applying a displacement on the top reference point.

Fig. 6. Heatmap with the knockdown factors based on linear buckling analyses.

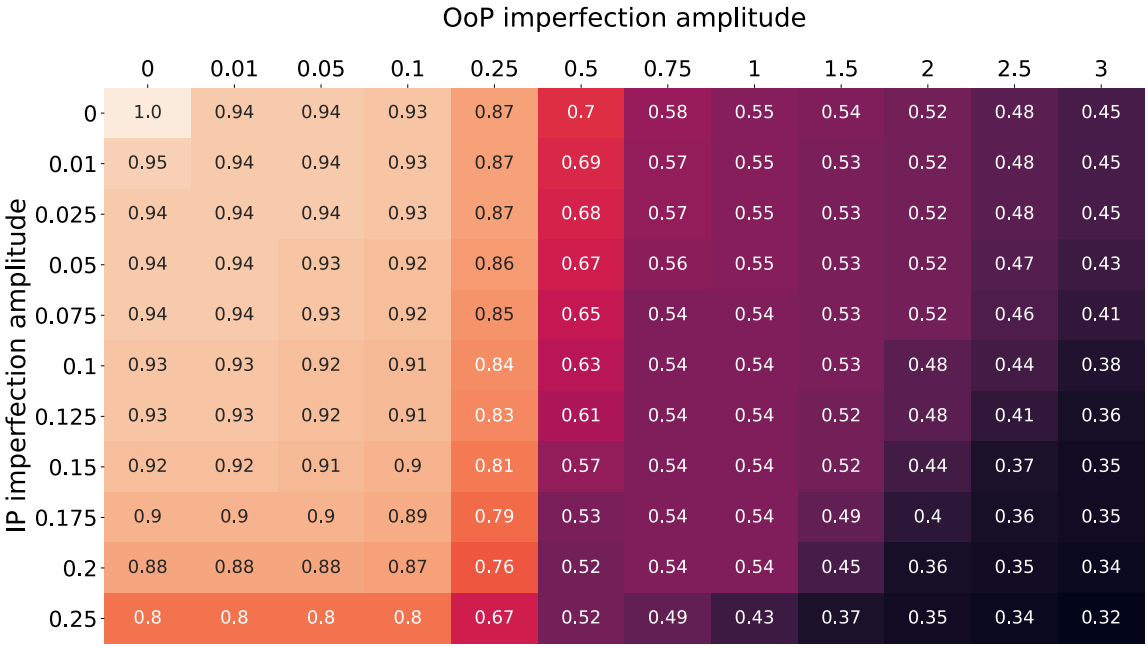

Fig. 7. Heatmap with the knockdown factors based on non-linear FE analyses.

Fig. 6 shows the knockdown factors based on linear buckling analyses, with respect to the value obtained from the model without imperfections (P_{cr} = 183.3 kN), for the various OoP imperfection amplitudes used. While for relatively small OoP amplitudes P_{cr} does not change much, the influence of the OoP imperfections becomes significant when an amplitude larger than 0.25 is used. Once this threshold amplitude is exceeded, these large differences are also bound to significantly change the VCT predictions and their influence was therefore investigated.

Fig. 7 shows the knockdown factors based on the non-linear analyses of the FE models with various amplitudes of OoP and IP imperfections with respect to the case without any imperfections, where P_{nl} = 182.8 kN. One important observation that offers perspective on the amplitudes of the IP imperfection used (0.25 — translating to a maximum displacement of 0.25 mm locally applied to the top and bottom cylinder edges) is that the buckling load for the FE model without imperfections was found at a displacement of 0.677 mm. This implies that, for the largest IP amplitude introduced, locally the edges of the cylinder shorten by a significant amount, roughly 0.5 mm, and can therefore be considered as a severe loading imperfection.

Upon analysing this figure, several aspects stand out. First, any small imperfection introduced has a significant influence over the buckling load, after which further increasing the amplitudes has a relatively minor influence until a certain threshold is reached. For the imperfection patterns used here, this threshold for the OoP imperfection amplitude seems to be after 0.1, while for the IP imperfection this seems to be after 0.175, the knockdown factors beyond these values significantly exceeding a value of 0.9. Second, after exceeding a certain OoP imperfection amplitude threshold, the influence of the loading imperfections starts to increase, resulting in a significant decrease in the buckling load. Furthermore, for any given OoP imperfection amplitude, there is an IP imperfection amplitude threshold after which the decrease in the buckling load tends to stabilise, and vice versa. The existence of these imperfection amplitude thresholds aligns with the findings of other studies where the imperfection amplitude was varied. One such example is the case where the lateral load/displacement is increased in the single load perturbation approach [3,63,70], where the buckling load decrease is severe within a certain interval of applied load/displacement, while outside this interval, the buckling load decrease is relatively small in comparison.

Increasing the amplitudes of the imperfections applied induced local buckling, associated with clear changes observed on the load–displacement curves. When local buckling occurred, it was initially related to a local dimple-like buckling pattern seen in the model's out of plane displacement field, dimple located roughly at the mid-height of the cylinder. Then, any additional local buckling events were either characterised by a change in the already existent localised buckling pattern, or by a similar pattern occurring roughly at the opposite side. When a change in the localised buckling pattern occurred, this implied that either an additional adjacent dimple-like pattern appeared next to the already existent one(s), along the circumference of the cylinder, or that a slight migration of the existent pattern occurred, also along the circumference of the cylinder. The frequency of these events generally increased with increasing the amplitudes of the imperfections, as shown in Fig. 8. In this regard, it appears that increasing the amplitude of the OoP imperfections is generally more significant in driving the apparition of local buckling. Nevertheless, once the threshold imperfection amplitudes leading to the occurrence of local buckling are exceeded, a clear evolution in the number of these load drops as a function of the applied IP and OoP imperfection amplitudes was not observed.

Fig. 9 shows the compressive response, in terms of load–displacement response, apparent stiffness, OoP displacement and the VCT load steps defined for a FE model where multiple load drops

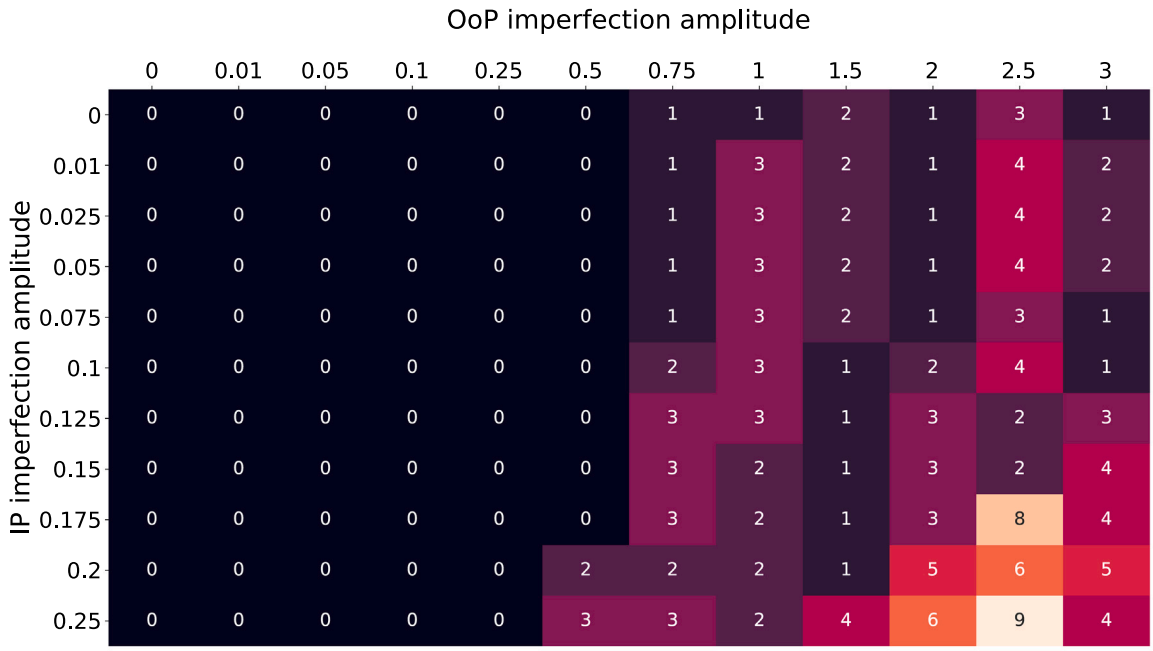

Fig. 8. Heatmap with the number of load-drops recorded.

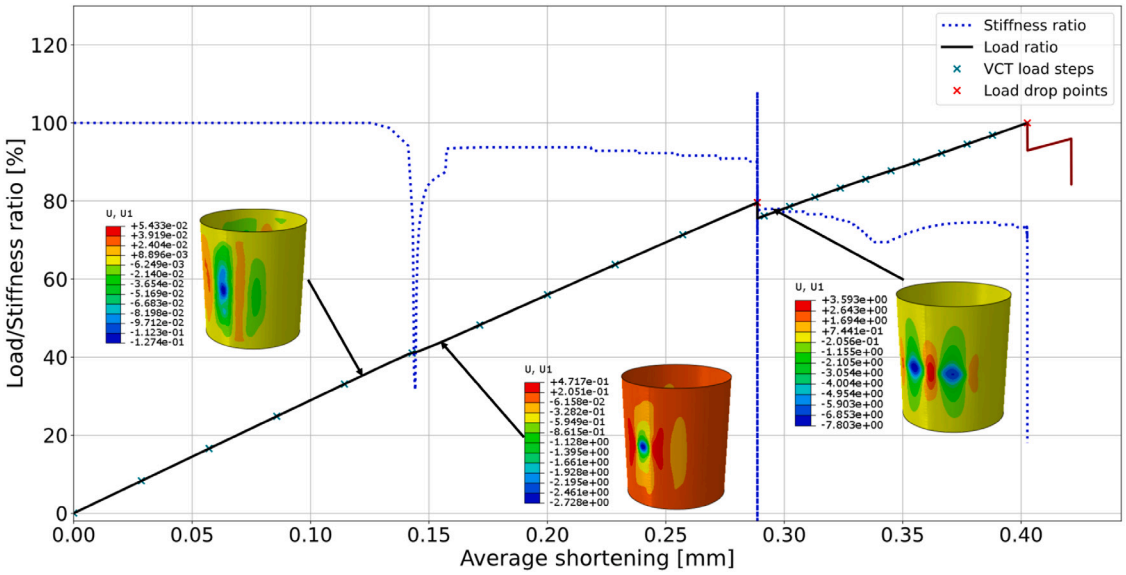

Fig. 9. Load ratio-displacement and stiffness ratio-displacement curves for IP = 0.125 and OoP = 1.5.

occurred before the maximum load level was reached (IP = 0.125, OoP = 1.5). In this plot, the load and stiffness were normalised with respect to the non-linear buckling load and initial stiffness, respectively, these values being shown in percentages. Given the loading imperfection introduced through uneven displacements applied to the top and bottom edge nodes, an average shortening was computed based on the axial displacements of these nodes. In this figure it can be seen that the introduced shape and loading imperfections favoured large localised OoP displacements, relative to other areas of the cylinder, located at its mid-height. As the load applied increased, in the area of large localised OoP displacements a clear, dimple-like, local buckling pattern developed, in the shown example this occurring roughly at 40% of P_{nl}. Then, around 80% of P_{nl}, a second local buckling occurred, with an additional dimple appearing next to the initial one. At P_{nl}, yet another dimple appeared in the localised buckling pattern, point after which increasing the applied axial displacement did not yield a higher reaction force.

As it can also be seen in this figure, there were cases where the VCT load steps were defined exclusively at high load ratios. It is important to mention that the authors acknowledge that load ratios as high as some of the ones defined in this study might represent too high of a risk to reach during an experimental test. Nonetheless, the VCT load steps at these high load ratios were kept here to investigate the predictive capabilities of VCT when load steps beyond the initial VCT regions are used. Furthermore, the authors also acknowledge that multiple load drops might not be found during an experimental test, especially if the load introduction is force-based, as local buckling might trigger the global buckling of the cylinder. Yet, although not very common, this behaviour can be found when the load introduction is displacement-based [3,14,15,55,71].

While the main reason for the stiffness monitoring was to decide, in the case where local buckling occurs, whether VCT load steps should be defined or not in the subsequent VCT regions, there was also an additional reason. This was to find any abrupt stiffness changes in the VCT regions which were not associated with load drops. Identifying these regions, like the ones shown in the above figure, was important in explaining some cases where none of the tracked vibration modes were found between consecutive load steps. When this behaviour was found, the results from the VCT steps at the higher load ratios were favoured.

3.2. VCT results

3.2.1. VCT imperfection sensitivity

Due to the different evolution of the vibration modes with the applied load and the occurrence of local buckling at different load ratios as a function of the applied imperfection amplitudes, a straight forward comparison between the results obtained was not possible. The different vibration mode evolution with the applied load for the different imperfection amplitudes meant that, in some cases, sufficient frequency entries were not found for the monitored vibration mode. On the other hand, the occurrence of local buckling at different load ratios for the different imperfection amplitudes applied would have demanded that the comparisons were made for load ratios as low as 30%, which are not recommended for robust VCT buckling load predictions. Therefore here, the averaged VCT buckling prediction errors of up to 15 vibration modes were compared, instead of prediction errors given by individual vibration modes. Furthermore, additional information, such as the variance of the averaged errors, the averaged maximum load ratios, the number of vibration modes used and the number of quasi-linear regions defined for each case, is provided. This additional information was deemed valuable for better understanding the results obtained and identifying the source of the differences found. The results are then shown in heatmaps for all the imperfection amplitudes, the heatmap cells being coloured as a function of the averaged errors.

Fig. 10(a) shows the averaged errors of the VCT predictions with respect to the global buckling load using load steps in the first VCT region, Arbelo's VCT procedure, P_{cr} for the perfect structure and a maximum load ratio of 70%. For understanding this figure, an example of the information contained in each cell is provided in Fig. 10(b). In this latter figure, the number in the red rectangle represents the averaged errors of the vibration modes used, value on which the heatmap cell colour is based. In the blue rectangle, the information on the VCT regions defined for that specific model is shown in the format x/y, where x represents the number of the VCT region for which the averaged errors are shown and y represents the number of VCT regions defined for that model. This information is useful when trying to understand the source of deviation for certain models when compared to others, as in some cases the VCT prediction might be poorer when multiple local buckling events occur. This can be the case especially if load steps before local buckling occur are used, since depending on the load level at which local buckling occurs, the maximum load ratio reached in that specific VCT region may be low. Furthermore, in the green rectangle the averaged maximum load ratios of the vibration modes used is shown. This information is also valuable when searching for the source of possible deviations, as in some cases the vibration modes could only be successfully monitored until a load ratio lower than the targeted one, therefore potentially having a significant influence on the VCT prediction error. In these cases, when the number of predictions within a load ratio tolerance of ±10% is lower than 4, the cell information is underscored to highlight this aspect. Last, in the purple rectangle information about the averaged errors is provided in the format $\sigma : x/y$, where x represents the variance of the averaged errors shown and y represents the number of vibration modes used. This was done to offer context for the averaged prediction errors and to the variance itself, since there is a risk of misinterpreting the results in absence of this additional information. More specifically, there is a chance of obtaining a low averaged error using exclusively large errors of opposite signs, or based solely on a few successful VCT predictions, which would lead to a severe misinterpretation on the result obtained.

Upon analysing Fig. 10(a) it can be seen that, as long as the averaged maximum load ratio for any given OoP and IP imperfection amplitudes is close to the targeted maximum load ratio, VCT tends to provide reliable buckling load predictions. This lack of correlation between the averaged errors and the imperfection amplitudes applied suggests that indeed VCT is generally insensitive to shape and loading imperfections, aspect also suggested by VCT tests on nominally identical cylinders [55]. Furthermore, even for some of the cases where the averaged load ratio was not close to the targeted one, mostly due to the occurrence of local buckling and outlined here by the underlines of the cell's content, the VCT predictions were still reliable. Nevertheless, when the maximum load ratio is outside the targeted one, the VCT predictions tend to be over-conservative, especially when large OoP and IP imperfections amplitudes were applied. Another important observation is that, for certain OoP imperfection amplitudes, specifically between 0.5 and 1, the VCT predictions tend to be consistently unconservative. While increasing the IP imperfection amplitude for these cases seems to alleviate this issue once a certain IP amplitude is exceeded, it remains a clear sign that certain OoP imperfection patterns may yield unconservative VCT predictions. VCT tests on nominally identical cylinders also showed that there are cases in which VCT can seriously overestimate the buckling load [55], here being shown that shape imperfections alone can be the source of this behaviour and that loading imperfections can also influence this aspect. Nevertheless, it was also noticed that these cases may be easily identified when performing a series of VCT predictions in which the load ratio used is gradually increased. The evolution of the predictions with the load ratio can then be monitored, which for the cases where these predictions are unconservative, the predictions are generally decreasing, rather than increasing. This aspect was also previously reported by the authors for several sets of experimental results in [72] and it was also observed for the aforementioned unconservative results.

After the imperfection amplitudes exceed a certain threshold, the variance of the averaged errors increased significantly, the only exceptions being for the cases where only a few vibration modes could be used. This increase in variance also meant that, for some vibration modes, the VCT predictions were far more accurate, with only 29 out of the total 132 (22%) cases giving an error larger than 10% when the best prediction for each case was chosen, most of them being for the largest OoP and IP imperfection amplitudes. Unfortunately, when different vibration modes yield largely different buckling load predictions, choosing the appropriate one beforehand during the experimental test is no easy task. In this regard, the quality of the second order fit was assessed, by averaging the distances between the points in the VCT characteristic chart and the fitted curve (also known as residuals). These averaged residuals for the averaged errors heatmap shown in Fig. 10(a) are shown in Fig. 11. For a better visualisation of these results, a factor of 1E4 was applied to the residuals. Furthermore, the number of predictions used in obtaining the averaged residuals is shown below to better understand these results and the possible differences between the different imperfection amplitudes.

As it can be seen when comparing the two figures aforementioned, such a criterion for choosing vibration modes is not recommended, given the lack of correlation between a robust VCT prediction and the residuals of the fitted curve. A clear decrease in the number of residuals used to compute the average can also be seen with increasing the imperfection amplitudes, particularly when increasing the OoP imperfection amplitude. This is because increasing the amplitude of the imperfections makes the structure more susceptible to vibration mode changes as the load increases, therefore some vibration modes could only be successfully tracked across a lower number of load steps.

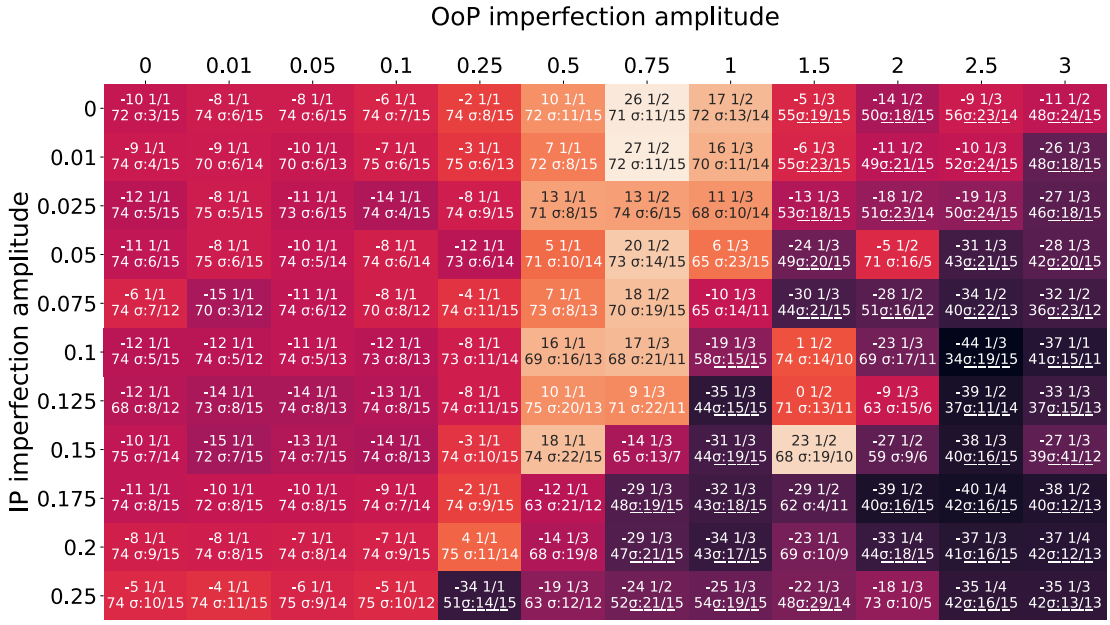

(a) Averaged errors heatmap for the initial VCT region for a load ratio up to 70%, using the analytical VCT formulation and P_{cr} of the pristine structure

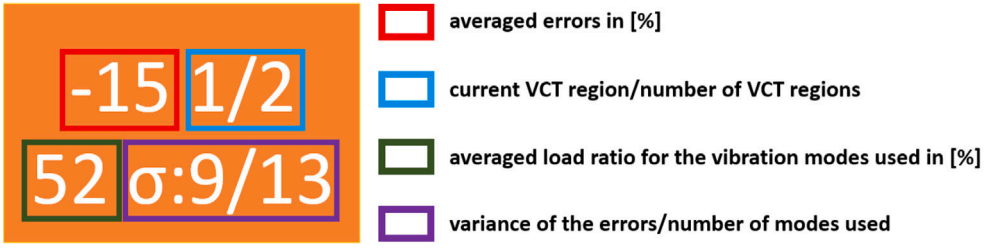

(b) Heatmap cell information example

Fig. 10. Averaged VCT prediction errors heatmap using load steps in the initial VCT region a) and heatmap cell information b)

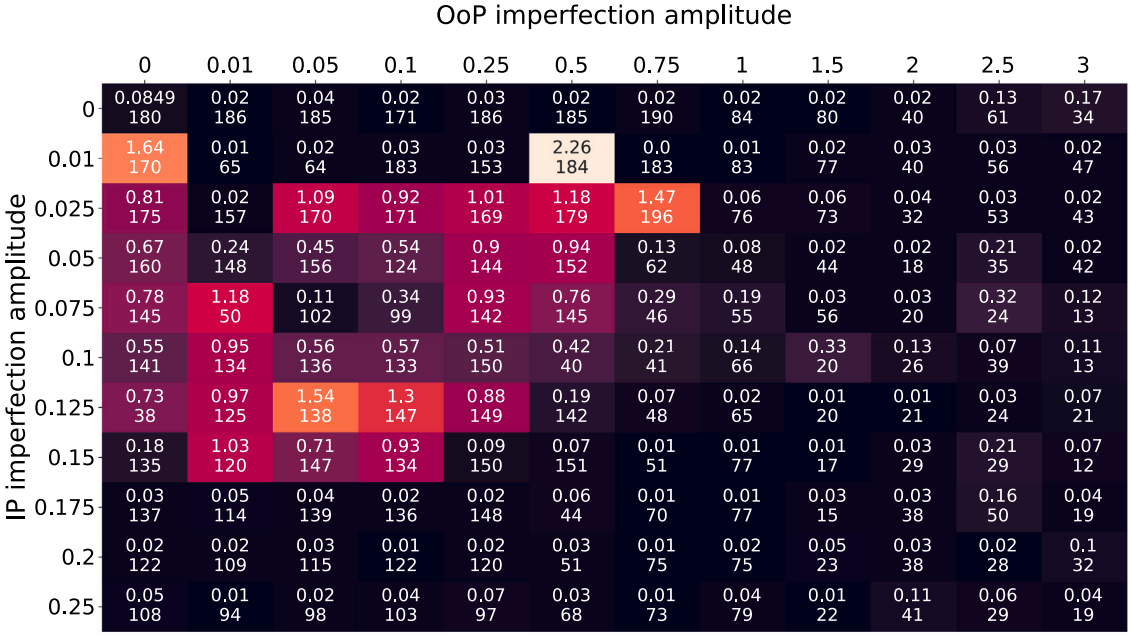

Fig. 11. Averaged residuals heatmap for the first VCT region, using the analytical VCT formulation and P_{cr} of the pristine structure.

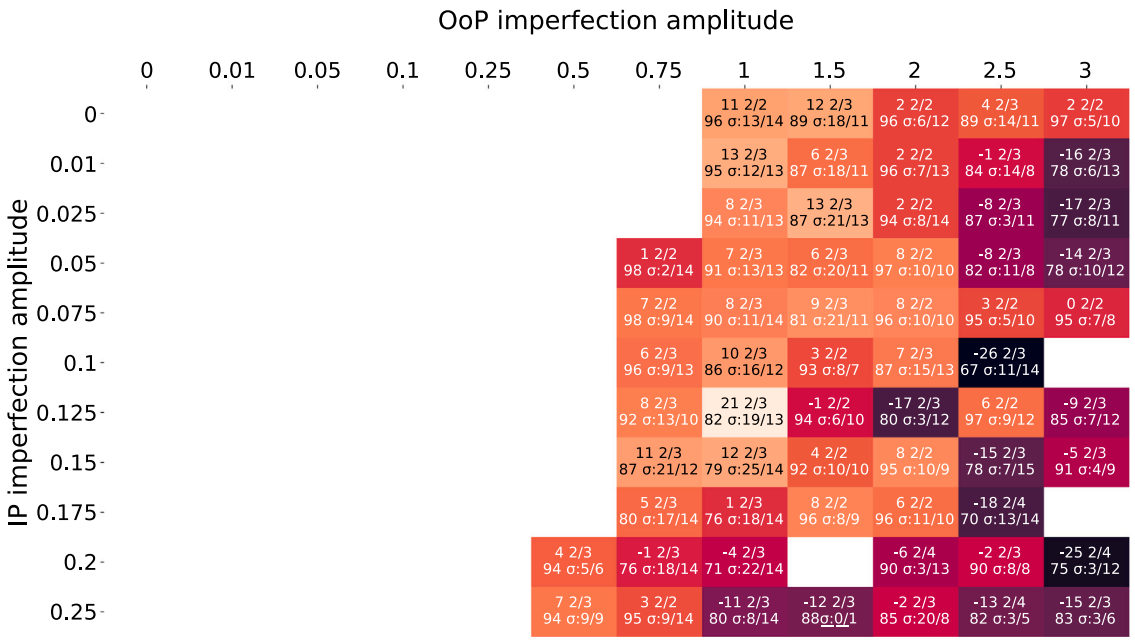

Fig. 12. Averaged errors heatmap for the second VCT region, using the analytical VCT formulation and P_{cr} of the pristine structure.

Fig. 12 shows the averaged errors with respect to the global buckling load using load steps in the second VCT region, using the same procedure as the one previously described for Fig. 10(a). Unlike for the initial VCT region, a target maximum load ratio was not set here, due to the various load ratios at the ends of each VCT region for the different imperfection amplitudes applied. Therefore, in this figure the underlined results are now highlighting the cases where less than 5 vibration modes could be successfully used to provide a VCT prediction.

Regarding the sensitivity of VCT to imperfections, the general trends observed for the initial VCT region, along with their exceptions, are also applicable here. Unlike in Fig. 10(a), a clear increase in the variance of the averaged errors with increasing the imperfection amplitudes is no longer observed. This is because the load ratios for which these VCT predictions were performed are more restricted, therefore these predictions are bound to have a lower variation. Perhaps the most important observation regarding the results based the second VCT region is the tendency of the predictions to be unconservative. Vibration modes that give accurate VCT predictions can also be found in this case, with 2 out of the 62 (3%) cases available providing an error larger than 10% when the vibration mode giving the best prediction was used. Nevertheless, same as for the initial VCT region, low quadratic curve fit residuals do not necessarily indicate a better prediction. Moreover, care must be taken when analysing these results, since the load levels used are all at relatively high load ratios, which inherently increases the likelihood of the prediction to be closer to the global buckling load. While vibration modes with a frequency response complying with the expected behaviour when applying VCT after an initial buckling occurs were found, the buckling load predictions using load steps in the VCT regions beyond the initial one tend to be unconservative, thus making them generally unreliable for the VCT procedure used here. Another important observation to be made here is that in some cases the frequency of certain vibration modes increased, rather than decreased, as the load applied increased. This behaviour appeared to be highly irregular, as the load after which this behaviour was noticed appeared to be dependent on the vibration mode and often not associated with a change in the model's apparent stiffness. Furthermore, there were also cases in which for a given vibration mode the frequency initially increased and then decreased after a certain load level was reached, while for other vibration modes the opposite was observed. Since a decrease of the vibration mode frequency is required to apply VCT, the load steps where an increase in the frequency of the vibration mode was observed were left out from the prediction using that specific mode.

3.2.2. VCT parameter study

In this study, an investigation was performed on the influence of P_{cr} and VCT method over the prediction accuracy and on whether the predictions for the cases with multiple VCT regions are closer to the local, or to the global, buckling load. This was done by comparing the averaged errors for each imperfection amplitudes when only the desired comparison parameter was changed and counting the occurrences where one case outperformed the other. For the purpose of discounting the cases where the difference between the compared parameters was relatively small, a tolerance of 5% was used to differentiate between the averaged errors compared. The investigation was also done across the other variables compared to identify whether there are certain combinations of VCT procedure, P_{cr} and error type that consistently provide robust predictions across all VCT regions. This resulted in 8 comparison cases for each of the parameters studied. Due to the large number of cases analysed, only an outline of the clear trends observed is given here, together with a discussion about these findings:

- Arbelo's analytical approach is best suited to be used in the initial VCT region when accuracy is desired
- The empirical VCT procedure tends to be more conservative than Arbelo's
- P_{cr} obtained for the perfect structure generally provides the best accuracy
- The empirical VCT procedure might be used in VCT regions beyond the initial one, when P_{cr} is obtained taking into account OoP imperfections

This provides valuable novel insight regarding the use of VCT to predict the in-situ buckling loads of cylindrical shells, since it gives a better understanding of its predictive capabilities. When trying to predict the global buckling load using load steps in the initial VCT region, Arbelo's analytical VCT method consistently gave the most accurate predictions, regardless of the P_{cr} values used, with the one for the perfect structure giving the best results. Similarly, P_{cr} for the perfect structure also seemed to provide the best results when predicting the global buckling load using Arbelo's procedure and load steps beyond the initial VCT region. When trying to predict the local buckling load using this method, it was noticed that these predictions were generally unconservative. Since using the P_{cr} with OoP imperfections taken into account generally lowers the predictions, using this value alleviated this

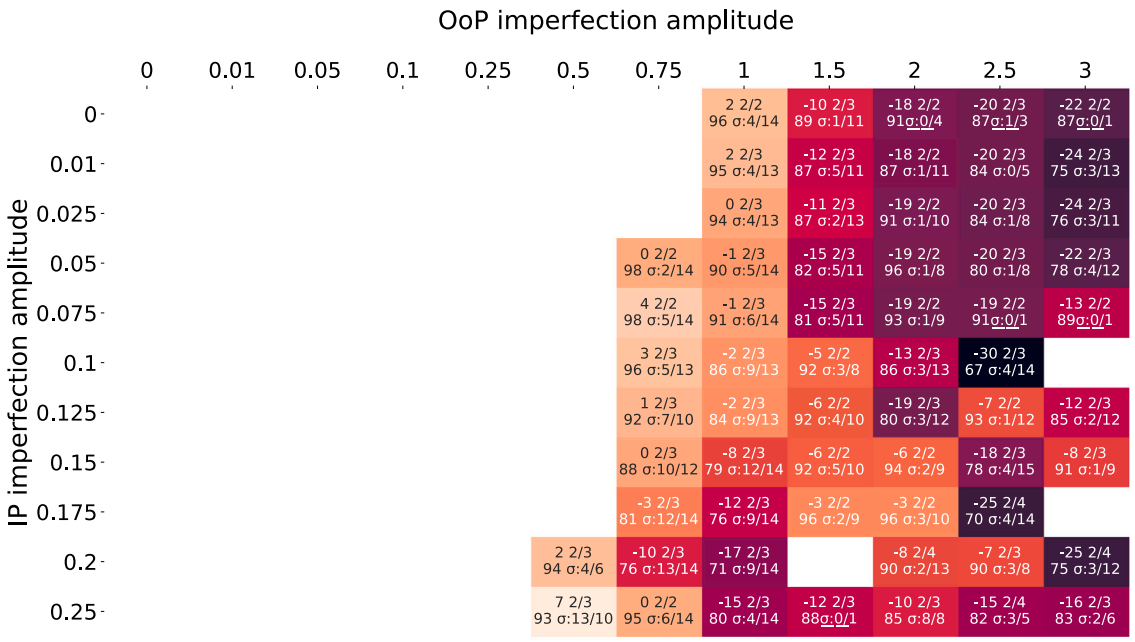

Fig. 13. Averaged errors heatmap for the second VCT region using the empirical VCT procedure and the P_{cr} taking into account OoP imperfections.

issue somewhat, but the predictions became over-conservative after a certain OoP imperfection amplitude was exceeded.

It was also noticed that the empirical VCT procedure was more conservative than the one proposed by Arbelo, aspect also reported in [55]. This represents the main reason why this method generally gave better local buckling predictions, particularly when OoP imperfections were taken into account in the buckling analysis. This procedure was also found to be better than Arbelo's method in predicting the global buckling load when using load steps beyond the initial local buckling. This was regardless of the P_{cr} used and the differences between this method and Arbelo's were only marginal, most likely due to the restricted load ratio intervals of the load steps defined in these VCT regions.

Fig. 13 shows the averaged VCT prediction errors with respect to the global buckling load using load steps in the second VCT region, where the empirical VCT procedure was employed, using the P_{cr} that takes into account the OoP imperfections. When comparing this figure with its counterpart Fig. 12, where P_{cr} for the perfect structure was used together with Arbelo's VCT procedure, a clear improvement regarding the unconservative predictions can be seen. Furthermore, the variance of the averaged errors is generally smaller, which can increase the confidence with regard to the obtained result. However, as previously mentioned, while using the P_{cr} that includes OoP imperfections can improve the unconservative predictions for some cases, it might also result in over-conservative predictions for others. While the overall accuracy is slightly lower than when the P_{cr} for the perfect structure was used, the more conservative nature of this approach is worth taking into account if predicting the global buckling load using load steps after local buckling has occurred is desired.

3.2.3. Experimental validation

The observations based on numerical investigations were also found to hold true in experimental VCT campaigns, namely the one conducted at Riga Technical University, on the robustness of the VCT procedure [56]. In this experimental campaign, several cylinders showed the same frequency response as the one observed for the numerical cases where local buckling was observed, namely a noticeable change in the frequency response of the cylinders as the load applied increased. Two of the cylinders tested and which showed the same frequency response change as the one observed in the numerical study as a result of local buckling occurring were selected for further investigation. These cylinders are labelled *D500H500L2N-02* and *D500H750L2N-01*, a more detailed description of the specimens, test procedure and frequency response being provided in the Appendix.

Fig. 14 shows the characteristic VCT chart using the analytical VCT method for the *D500H750L2N-01* cylinder, where the initial load step was neglected, due to inconsistent boundary conditions at insignificant load ratios.

Here progressive quadratic fits were performed by incrementally increasing the load ratio, highlighting the targeted value corresponding to the experimental buckling load and providing the load ratios on the right vertical axis. Here it can be clearly seen that there is a significant change in the frequency response of the cylinder happening between a 40% and a 51% load ratio and therefore the VCT load steps were split into two VCT regions. Furthermore, it can also be seen that after this change occurred, it rendered the progressive predictions, starting from the 12th and up to the 19th VCT load step, unsuccessful. Once the successful progressive predictions resumed, it can also be seen that these decreased with increasing the load ratio, diverging thus from the general behaviour. A very similar behaviour was also observed for cylinder *D500H500L2N-02*, the only difference being that, due to the smaller nature of the frequency response change, all the progressive quadratic fits after this point were successful.

Figs. 15(a) and 15(b) show the relative prediction errors with respect to the experimental buckling loads for the *D500H500L2N-02* and *D500H750L2N-01* cylinders. In these figures the curves in black represent the progressive VCT predictions using all the load steps, while the ones in dark red represent the progressive VCT predictions using only the load steps in the second VCT regions. Similarly, the solid lines represent the VCT predictions using the analytical method, while the dashed lines represent the predictions using the empirical one.

By examining these figures and comparing the solid lines against their dashed counterparts, one can observe that the latter tend to be lower in most cases, highlighting the more conservative nature of the empirical method when compared to the analytical one. Furthermore, the likelihood of the empirical method to yield more successful predictions can also be noticed upon a closer inspection, giving the larger number of points on the dashed curves when compared to their counterparts. Using the load steps after a change occurred in the frequency response of the cylinders yielded successful predictions for all the load steps available, regardless of the VCT method used, and were more robust with respect to the analytical method where all the available load steps were used. On the other hand, a better accuracy overall was not achieved for the *D500H500L2N-02* cylinder, the empirical method

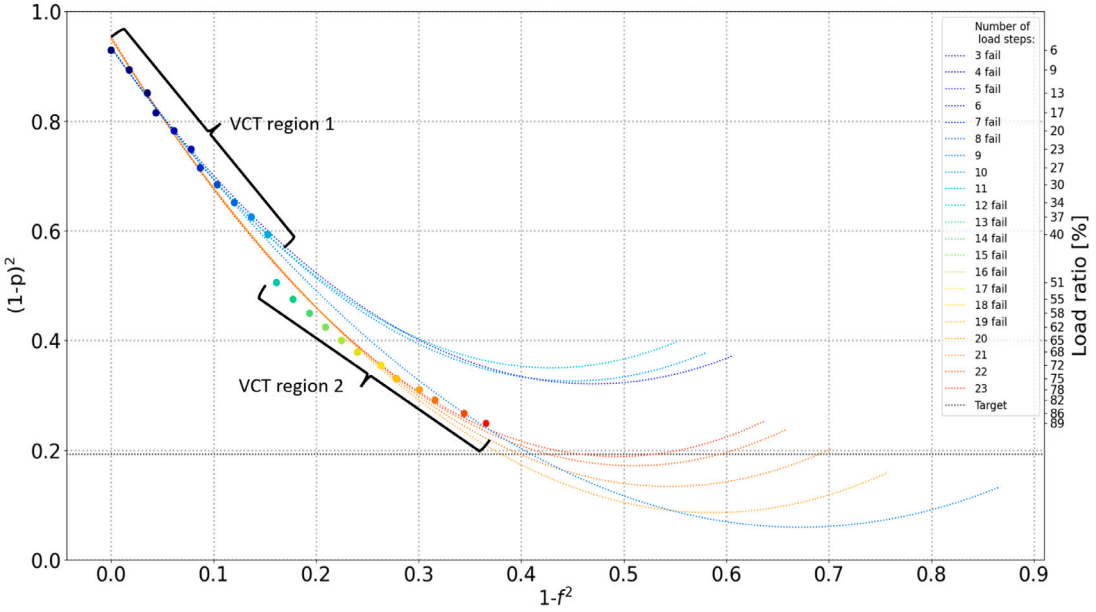

Fig. 14. D500H750L2N-01 VCT characteristic chart, analytical method.

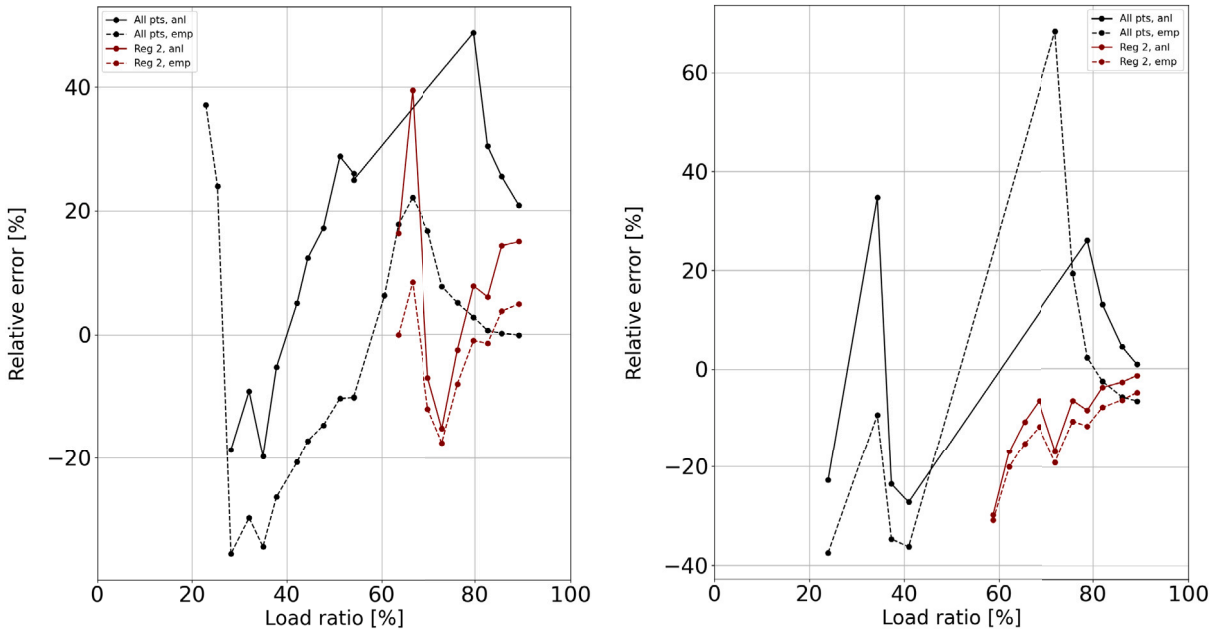

(a) D500H500L2N-02 (b) D500H750L2N-01

Fig. 15. Relative VCT buckling load prediction error with respect to the experimental buckling load of the analytical and the empirical VCT methods for the D500H500L2N-02 and D500H750L2N-01 cylinders.

using all the load steps available giving the best prediction. The best overall accuracy for the *D500H750L2N-01* was also achieved using all the load steps available, but using the analytical method, the prediction being also slightly unconservative. When compared to the numerical results, the general trend was more similar to the one observed for the *D500H750L2N-01* cylinder, using the load steps after the change in the frequency response generally giving better VCT buckling load estimations.

4. Conclusions

In this paper, the capability of the VCT to predict buckling of cylindrical shells under axial compression with various shape and loading imperfection amplitudes was investigated. Furthermore, whether OoP imperfections should be taken into account when computing the value of P_{cr} or whether, in the event of local buckling occurring, VCT better predicts the local, rather than the global, buckling load was also investigated for two VCT procedures.

It was found that VCT tends to be relatively insensitive to shape and loading imperfections, as a clear trend regarding the accuracy of the averaged prediction errors as a function of the applied imperfection amplitudes was not observed. This aspect is also supported by the large number of experimental tests in which VCT provided robust global buckling load predictions [19,44–56]. It was also found that certain shape imperfections might alter both the accuracy and the general conservatives of the VCT buckling load predictions. However, for these cases, usually the VCT predictions tend to decrease, rather than increase, with increasing the load ratio, making the detection of this

behaviour easy to identify by performing a series of VCT predictions in which the maximum load ratio is gradually increased.

When no local buckling occurs, Arbelo's method in which P_{cr} for the perfect structure was used consistently gave the best results. Furthermore, while the global buckling load predictions using this procedure and load steps beyond the initial local buckling were less accurate than the predictions provided by the empirical method, the difference between the two VCT procedures in this regard were mostly marginal. Same as for the initial VCT region, the P_{cr} for the perfect structure also seemed to provide the best results in this case.

When the averaged errors were compared against the local buckling loads, the predictions using Arbelo's VCT method and the P_{cr} for the perfect structure were often unconservative and inconsistent across the multiple imperfection amplitudes used. Using the empirical VCT procedure and taking into account the shape imperfections when computing P_{cr} seemed to improve the predictions for some imperfection amplitudes, but resulted in over-conservative prediction for large imperfection amplitudes. Therefore, in the event of local buckling occurring, the authors do not recommend using VCT to predict the load at which local buckling occurs.

The numerical results shown here suggest that predicting the global buckling using load steps after local buckling occurs might be possible. However, it was observed that the now established VCT procedure proposed by Arbelo, and in which the P_{cr} for the perfect structure is used, often gives unconservative predictions. Including the shape imperfections in the buckling analysis and using the empirical VCT procedure seemed to be more reliable in this regard, as the averaged errors became more conservative and their variance also decreased. Analyses using experimental data also confirmed most of the numerically observed trends. Using the VCT measurements of two cylinders under axial compression for which a sudden change in frequency response was observed, the feasibility of robust VCT buckling load predictions using load steps after a change in the frequency response occurred was shown. Furthermore, the more conservative nature of the empirical method with respect to the analytical one was also clearly seen on the analyses based on experimental data, same as the tendency of these changes in frequency response to alter the robustness of the VCT predictions. For these two cases, when all the load steps were used, the change in the frequency response triggered a decrease of the VCT buckling load prediction with increasing the load ratio and rendered several predictions after that point unsuccessful. On the other hand, using load steps exclusively after the change in the frequency response occurred yielded VCT buckling load predictions more robust with respect to the ones obtained using all the load steps and the analytical VCT procedure, predictions which were also generally increasing with the maximum load ratio used.

CRediT authorship contribution statement

T.D. Baciu: Conceptualization, Data curation, Formal analysis, Investigation, Methodology, Resources, Software, Validation, Visualization, Writing – original draft, Writing – review & editing. **F. Franzoni:** Data curation, Resources, Software, Supervision, Visualization, Writing – review & editing. **R. Degenhardt:** Funding acquisition, Project administration, Supervision, Writing – review & editing. **K. Kalnins:** Funding acquisition, Investigation, Resources, Writing – review & editing. **C. Bisagni:** Supervision, Writing – review & editing.

Declaration of competing interest

The authors declare that they have no known competing financial interests or personal relationships that could have appeared to influence the work reported in this paper.

Data availability

Data will be made available on request.

Appendix. D500H500L2N-02 and D500H750L2N-01 cylinders experimental data

The D500H500L2N-02 and D500H750L2N-01 cylinders were part of an extensive experimental campaign on the robustness of VCT to predict the buckling loads of unstiffened composite cylindrical shells under axial compression, conducted at Riga Technical University. The diameter, height, linear (perfect cylinder) and experimental buckling loads of these two cylinders are shown in Table 2. The material used was a Unipreg uni-directional prepreg, with a lamina thickness of 1.044 mm and the averaged, strain-gauge measured, material properties shown in Table 3, where the *T/C* subscripts stand for *Tension/Compression*. The manufacturing of the cylinders was done by hand lay-up using steel mandrels and then initially curing them in vacuum bags for one hour at a temperature 80 °C and then for an additional three hours at a temperature of 130 °C [55].

The cylinders were tested on a Zwick Z100 quasi-static testing machine, with a displacement loading rate of 1 mm per minute. The load was introduced by parallel plates, the load being recorded by the testing machine's loading cell. To measure the cylinder's shortening, the measurements of three LVDT's equally spaced across the cylinder's circumference were averaged. The cylinder's vibration response was measured by a Polytec laser vibrometer, the frequencies of the modes measured and their afferent loads being shown in Table 4.

Table 2
D500H500L2N-02 and *D500H750L2N-01* cylinders geometry, linear and experimental buckling loads.

D500H500L2N-02		D500H750L2N-01	
D = 500 [mm]	H = 500 [mm]	D = 500 [mm]	H = 750 [mm]
P_{cr} = 16.54 [kN]	P_{exp} = 10.47 [kN]	P_{cr} = 17.02 [kN]	P_{exp} = 9.65 [kN]

Table 3
Unipreg material properties [46].

E_{1T}	E_{1C}	E_{2T}	E_{2C}	G_{12}	ν_{12}
116.44 [GPa]	91.65 [GPa]	6.73 [GPa]	6.39 [GPa]	3.63 [GPa]	0.34

Table 4
D500H500L2N-02 and D500H750L2N-01 cylinders load-frequency response.

D500H500L2N-02		D500H750L2N-01	
Load [kN]	Frequency [Hz]	Load [kN]	Frequency [Hz]
0	174.5	0	113.5
0.356	173.5	0.616	113
0.654	172	0.938	112
1.003	171	1.33	111
1.354	169.5	1.668	110.5
1.668	168.5	1.981	109.5
1.991	167	2.313	108.5
2.398	165.5	2.656	108
2.654	164.5	2.972	107
2.952	163	3.313	106
3.353	161.5	3.6	105
3.659	160	3.949	104
3.957	159	4.97	103.5
4.413	157	5.337	102.5
4.65	156	5.666	101.5
4.992	154.5	5.995	100.5
5.359	153	6.309	99.5
5.663	151.5	6.614	98.5
5.917	151.5	6.958	97
6.344	149.5	7.316	96
6.658	148	7.611	94.5
6.971	146.5	7.913	93.5
7.34	144.5	8.309	91.5
7.651	142.5	8.612	90
7.992	141		
8.347	139		
8.654	137		
8.963	135.5		

References

[1] Hilburger MW. Buckling of thin walled circular cylinders, NASA/SP-8007-2020/REV 2. NASA Langley Research Center; 2020, URL https://ntrs.nasa.gov/citations/20205011530.

[2] Degenhardt R, Kling A, Bethge A, Orf J, Kärger L, Zimmermann R. Investigations on imperfection sensitivity and deduction of improved knock-down factors for unstiffened CFRP cylindrical shells. Compos Struct 2010;92(8):1939–46. http://dx.doi.org/10.1016/j.compstruct.2009.12.014.

[3] Castro SGP, Zimmermann R, Arbelo MA, Khakimova R, Hilburger MW, Degenhardt R. Geometric imperfections and lower-bound methods used to calculate knock-down factors for axially compressed composite cylindrical shells. Thin-Walled Struct 2014;74:118–32. http://dx.doi.org/10.1016/j.tws.2013.08.011.

[4] Kepple J, Herath M, Pearce G, Prusty G, Thomson R, Degenhardt R. Improved stochastic methods for modelling imperfections for buckling analysis of composite cylindrical shells. Eng Struct 2015;100:385–98. http://dx.doi.org/10.1016/j.engstruct.2015.06.013.

[5] Southwell RV. On the general theory of elastic stability. Philos Trans R Soc A 1914;213:187–244. http://dx.doi.org/10.1098/rsta.1914.0005.

[6] Broggi M, Schuëller GI. Efficient modeling of imperfections for buckling analysis of composite cylindrical shells. Eng Struct 2011;33(5):1796–806. http://dx.doi.org/10.1016/j.engstruct.2011.02.019.

[7] Ansari QM, Trinh LC, Zucco G, Weaver PM. Effect of elastic support on the linear buckling response of quasi-isotropic cylindrical shells under axial compression. Eng Struct 2021;244:112796. http://dx.doi.org/10.1016/j.engstruct.2021.112796.

[8] Lopes CS, González C, Falcó O, Naya F, LLorca J, Tijs B. Multiscale virtual testing: the roadmap to efficient design of composites for damage resistance and tolerance. CEAS Aeronaut. J. 2016;7:607–19. http://dx.doi.org/10.1007/s13272-016-0210-7.

[9] Müzel SD, Bonhin EP, Guimarães NM, Guidi ES. Application of the finite element method in the analysis of composite materials: A review. Polymers 2020;12. http://dx.doi.org/10.3390/polym12040818.

[10] Chaves-Vargas M, Dafnis A, Reimerdes HG, Schröder KU. Modal parameter identification of a compression-loaded cfrp stiffened plate and correlation with its buckling behaviour. Prog Aerosp Sci 2015;8:39–49. http://dx.doi.org/10.1016/j.paerosci.2015.05.009.

[11] Kepple J, Herath MT, Pearce G, Prusty BG, Thomson R, Degenhardt R. Stochastic analysis of imperfection sensitive unstiffened composite cylinders using realistic imperfection models. Compos Struct 2015;126:159–73. http://dx.doi.org/10.1016/j.compstruct.2015.02.063.

[12] Wang B, Du K, Hao P, Zhou C, Tian K, Xu S, et al. Numerically and experimentally predicted knockdown factors for stiffened shells under axial compression. Thin-Walled Struct 2016;109:13–24. http://dx.doi.org/10.1016/j.tws.2016.09.008.

[13] Franzoni F, Degenhardt R, Albus J, Arbelo MA. Numerical assesment of existing vibration correlation technique. Compos Struct 2018;210:446–57, URL https://elib.dlr.de/124717/.

[14] Jiao P, Chen Z, Xu F, Tang X, Su W. Effects of ringed stiffener on the buckling behavior of cylindrical shells with cutout under axial compression: experimental and numerical investigation. Thin-Walled Struct 2018;123:232–43. http://dx.doi.org/10.1016/j.tws.2017.11.013.

[15] Wagner HNR, Hühne C, Janssen M. Buckling of cylindrical shells under axial compression with loading imperfections: An experimental and numerical campaign on low knockdown factors. Thin-Walled Struct 2020;151:106764. http://dx.doi.org/10.1016/j.tws.2020.106764.

[16] Jiao P, Chen Z, Ma H, Ge P, Gu Y, Miao H. Buckling behaviors of thin-walled cylindrical shells under localized axial compression loads, Part 2: numerical study. Thin-Walled Struct 2021;169:108330. http://dx.doi.org/10.1016/j.tws.2021.108330.

[17] Tian K, Huang L, Sun Y, Zhao L, Gao T, Wang B. Combined approximation based numerical vibration correlation technique for axially loaded cylindrical shells. Eur J Mech / A Solids 2022;93:104553. http://dx.doi.org/10.1016/j.euromechsol.2022.104553.

[18] Hu R, Wang W, Zhang C. Effect of preloading on vibration and buckling responses of variable stiffness composite cylindrical shells. Eng Struct 2023;287:116193. http://dx.doi.org/10.1016/j.engstruct.2023.116193.

[19] Arbelo MA, de Almeida SFM, Donadon M, Rett SR, Degenhardt R, Castro SGP, et al. Vibration correlation technique for the estimation of real boundary conditions and buckling load of unstiffened plates and cylindrical shells. Thin-Walled Struct 2014;79:119–28. http://dx.doi.org/10.1016/j.tws.2014.02.006.

[20] Li W, Fan H. Free vibration behaviors and vibration correlation technique of hierarchical isogrid stiffened composite cylinders. Thin-Walled Struct 2021;159:107321. http://dx.doi.org/10.1016/j.tws.2020.107321.

[21] Somerfeld A. Eine einfache vorrichtung zur veranschaulichung des knickungsvorganges. Z Ver Dtsch Ing 1905;49:1320–3.

[22] Melan H. Kritische drehzahlen von wellen mit langsbelastung. Z Osterr Ingenieur-Architekten-Vereines 1917;69. 610-612, 619-621.

[23] Ban S. Über die knicklast und die eigenschwingungszahl eines längsbelasteten stabes. Memoirs Coll Eng, Kyoto Imperial Univ 1931;4(4):275–91, URL http://hdl.handle.net/2433/280112.

[24] Engler W. Untersuchung der Knickfestigkeit und des Einspannungsverbältnisses von Balken auf dynamischem Wege. 1922.

[25] Föppl L. Bestimmung der knicklast eines stabes aus schwingungsversuchen. In: Beiträge zur technischen Mechanik und technischen Physik. 1924, p. 82–8. http://dx.doi.org/10.1007/978-3-642-51983-3.

[26] Engler W. Eine neue methode zur untersuchung der knickfestigkeit und des einspannungsgrads. In: Der Bauingenieur. 1926, p. 343.

[27] Grauers H. Transversalschwingungen rechteckiger platten mit besonderer rücksicht der knickung. In: Ingeniörs vetenskaps akademiens: handlingar, Nr. 98 Svenska Bokhandelscentralen. 1929.

[28] Schaefer H, Havers A. Die eigenschwingungen der in ihrer Ebene allseitig gleichmäßig belasteten gleichseitigen Dreiecksplatte. Ingenieur-Archiv 1936;7(1):83–7. http://dx.doi.org/10.1007/BF02084138.

[29] Stephens BC. Natural vibration frequencies of structural members as an indication of end fixity and magnitude of stress. J Aeronaut Sci 1936;4(2):54–60. http://dx.doi.org/10.2514/8.321.

[30] Penzes LE. Effect of boundary conditions on flexural vibrations of thin orthogonally stiffened cylindrical shells. J Acoust Soc Am 1967;42(4):901–3. http://dx.doi.org/10.1121/1.1910668.

[31] Chailleux A, Hans Y, Verchery G. Experimental study of the buckling of laminated composite columns and plates. Int J Mech Sci 1975;17(8):489–98. http://dx.doi.org/10.1016/0020-7403(75)90013-2.

[32] Massonnet CE. Les relations entre les modes normaux de vibration et la stabilité des systèmes élastiques. Bull Cours Lab d'Essais Constr Génie Civ d'Hydraulique Fluviale 1940;1(1-2).

[33] Massonnet CE. Le voilement des plaques planes sollicitées dans leur plan. In: Final report of the 3rd congress of the international association for bridge and structural engineering. 1948, http://dx.doi.org/10.5169/seals-4088.

[34] Lurie H. Lateral vibrations as related to structural stability. ASME J Appl Mech 1952;19:195–204. http://dx.doi.org/10.1115/1.4010446.

[35] Johnson EE, Goldhammer BF. The determination of the critical load of a column or stiffened panel by the vibration method. Proc Soc Exp Stress Anal 1953;11:221–32.

[36] Bassily SF, Dickenson SM. Buckling and lateral vibration of rectangular plates subject to inplane loads-a ritz approach. J Sound Vib 1972;24(2):219–39. http://dx.doi.org/10.1016/0022-460X(72)90951-0.

[37] Bozich WF. Technical report AFFDL-TR-67-28, The vibration and buckling characteristics of cylindrical shells under axial load and external pressure. USAF, Air Force Flight Dynamics Lab Wright-Patterson, Air Force Base Ohio, Vehicle Dynamics Division; 1967, URL https://apps.dtic.mil/sti/pdfs/AD0656302.pdf.

[38] Thielmann W, Garkisch HD. Einfluss von schiiringungen auf die beullast dunnwandiger kreiszylinderschalen. Braunschweig: DFL Bericht; 1965.

[39] Ponsford HT. The effects of stiffness on the buckling of cylinders with moderate wall thickness [Ph.D. Dissertation], California Institute of Technology; 1953, http://dx.doi.org/10.7907/JAYX-PF29.

[40] Fung YG, Kaplan A, Sechler EE. Experiments on the vibration of thin cylindrical shells under internal pressure. The Ramo-Wooldridge Corporation, Guided Missile Research Division; 1955, URL https://apps.dtic.mil/sti/pdfs/AD0607517.pdf.

[41] Okubo S, Whittier JS. A note on buckling and vibrations of an externall pressurized shallow spherical shell. J Appl Mech 1967;34(4):1032–4.

[42] Radhakrishnan R. Prediction of buckling strengths of cylindrical shells from their natural frequencies. Earthq Eng Struct Dyn 1973;2:107–15. http://dx.doi.org/10.1002/eqe.4290020202.

[43] Rosen A, Singer J. Vibrations of axially loaded stiffened cylindrical shells. J Sound Vib 1974;34(3):357–78. http://dx.doi.org/10.1016/S0022-460X(74)80317-2.

[44] Franzoni F, Degenhardt R, Albus J, Arbelo MA. Vibration correlation technique for predicting the buckling load of imperfection-sensitive isotropic cylindrical shells: an analytical and numerical verification. Thin-Walled Struct 2019;140:236–47. http://dx.doi.org/10.1016/j.tws.2019.03.041.

[45] Arbelo MA, Castro SGP, Khakimova R, Degenhardt R. Improving the correlation of finite element models using vibration correlation technique on composite cylindrical shells. In: 54th Israel Annual Conference on Aerospace Sciences, Tel-Aviv and Haifa, vol. 1, 2014, p. 453–9.

[46] Arbelo MA, Kalnins K, Ozoliņš O, Skukis E, Castro SGP, Degenhardt R. Experimental and numerical estimation of buckling load on unstiffened cylindrical shells using a vibration correlation technique. Thin-Walled Struct 2015;94:273–9. http://dx.doi.org/10.1016/j.tws.2015.04.024.

[47] Arbelo MA, Herrmann A, Castro SGP, Khakimova R, Zimmermann R, Degenhardt R. Investigation of buckling behavior of composite shell structures with cutouts. Appl Compos Mater 2015;22:623–36. http://dx.doi.org/10.1007/s10443-014-9428-x.

[48] Skukis E, Kalnins K, Ozoliņš O. Application of vibration correlation technique for open hole cylinders. In: Proceedings of the 5th International Conference on Nonlinear Dynamics, Kharkov, September 27-30, vol. 5, 2016, p. 377–83, URL http://repository.kpi.kharkov.ua/handle/KhPI-Press/24830.

[49] Skukis E, Ozoliņš O, Andersons J, Kalnins K, Arbelo MA. Applicability of the vibration correlation technique for estimation of the buckling load in axial compression of cylindrical isotropic shells with and without circular cutouts. Shock Vib 2017;5:377–83. http://dx.doi.org/10.1155/2017/2983747.

[50] Franzoni F, Odermann F, Wilckens D, Skukis E, Kalnins K, Arbelo MA, et al. Assessing the axial buckling load of a pressurized orthotropic cylindrical shell through vibration correlation technique. Thin-Walled Struct 2019;137:353–66. http://dx.doi.org/10.1016/j.tws.2019.01.009.

[51] Kalnins K, Arbelo MA, Ozoliņš O, Skukis E. Experimental nondestructive test for estimation of buckling load on unstiffened cylindrical shells using vibration correlation technique. Shock Vib 2015;2015. http://dx.doi.org/10.1155/2015/729684.

[52] Labans E, Abramovich H, Bisagni C. An experimental vibration-buckling investigation on classical and variable angle tow composite shells under axial compression. J Sound Vib 2019;449:315–29. http://dx.doi.org/10.1016/j.jsv.2019.02.034.

[53] Shahgholian-Ghahfarokhi D, Rahimi G. Buckling load prediction of grid-stiffened composite cylindrical shells using the vibration correlation technique. Compos Sci Technol 2018;167:470–81. http://dx.doi.org/10.1016/j.compscitech.2018.08.046.

[54] Shahgholian-Ghahfarokhi D, Rahimi G, Liaghat G, Franzoni F, Degenhardt R. Buckling prediction of composite lattice sandwich cylinders (CLSC) through the vibration correlation technique (VCT): Numerical assessment with experimental and analytical verification. Composites Part B: Eng 2020;199. http://dx.doi.org/10.1016/j.compositesb.2020.108252.

[55] Skukis E, Jekabsons G, Andersons J, Ozoliņš O, Labans E, Kalnins K. Robustness of empirical vibration correlation techniques for predicting the instability of unstiffened cylindrical composite shells in axial compression. Polymers 2020;12. http://dx.doi.org/10.3390/polym12123069.

[56] Skukis E, Jekabsons G, Ozoliņš O, Kalnins K. VCT vibration correlation technique for assessment of structural load bearing capacity. Institute of Material and Technology Riga Technical University; 2020, URL http://vct.rtu.lv/results.html.

[57] Jeon MH, Cho HJ, Sim CH, Kim YJ, Lee MY, Kim IG, et al. Experimental and numerical approach for predicting global buckling load of pressurized unstiffened cylindrical shells using vibration correlation technique. Compos Struct 2023;305:116460. http://dx.doi.org/10.1016/j.compstruct.2022.116460.

[58] Tian K, Huang L, Sun Y, Du K, Hao P, Wang B. Fast buckling load numerical prediction method for imperfect shells under axial compression based on pod and vibration correlation technique. Compos Struct 2020;252:112721. http://dx.doi.org/10.1016/j.compstruct.2020.112721.

[59] Tian K, Huang L, Sun Y, Yang M, Hao P, Wang B. Concurrent numerical implementation of vibration correlation technique for fast buckling load prediction of cylindrical shells under combined loading conditions. Eng Comput 2021;38:3269–81. http://dx.doi.org/10.1007/s00366-021-01458-9.

[60] Dassault Systèmes Simulia. Abaqus Unified FEA, Available online: https://www.3ds.com/products-services/simulia/products/abaqus/.

[61] Labans E, Bisagni C. Buckling and free vibration study of variable and constant-stiffness cylindrical shells. In: European conference on spacecraft structures, materials and environmental testing. (ECSSMET), 2018, http://dx.doi.org/10.1016/j.compstruct.2018.11.061.

[62] Wang B, Zhu S, Hao P, Bi X, Du K, Chen B, et al. Buckling of quasi-perfect cylindrical shell under axial compression: A combined experimental and numerical investigation. Int J Solids Struct 2018;130–131:232–47. http://dx.doi.org/10.1016/j.ijsolstr.2017.09.029.

[63] Jiao P, Chen Z, Tang X, Su W, Wu J. Design of axially loaded isotropic cylindrical shells using multiple perturbation load approach – simulation and validation. Thin-Walled Struct 2018;133:1–6. http://dx.doi.org/10.1016/j.tws.2018.09.028.

[64] Holst JMFG, Rotter JM. Axially compressed cylindrical shells with local settlement. Thin-Walled Struct 2005;43(5):811–25. http://dx.doi.org/10.1016/j.tws.2004.10.011.

[65] Błachut J. Buckling of axially compressed cylinders with imperfect length. Comput Struct 2010;88(5-6):365–74. http://dx.doi.org/10.1016/j.compstruc.2009.11.010.

[66] Cao Q, Zhao Y. Buckling strength of cylindrical steel tanks under harmonic settlement. Thin-Walled Struct 2010;48(6):391–400. http://dx.doi.org/10.1016/j.tws.2010.01.011.

[67] Kriegesmann B, Hilburger M, Rolfes R. The effects of geometric and loading imperfections on the response and lower-bound buckling load of a compression-loaded cylindrical shell. In: 53rd AIAA/ASME/ASCE/AHS/ASC structures, structural dynamics and materials conference. 2012, http://dx.doi.org/10.2514/6.2012-1864.

[68] Chen Z, Fan H, Cheng, Jiao P, Xu F, Zheng C. Buckling of cylindrical shells with measured settlement under axial compression. Thin-Walled Struct 2018;123:351–9. http://dx.doi.org/10.1016/j.tws.2017.11.006.

[69] Wagner HNR, Hühne C, Niemann S, Khakimova R. Robust design criterion for axially loaded cylindrical shells - simulation and validation. Thin-Walled Struct 2017;115:154–62. http://dx.doi.org/10.1016/j.tws.2016.12.017.

[70] Khakimova R, Castro SGP, Wilckens D, Rohwer K, Degenhardt R. Buckling of axially compressed CFRP cylinders with and without additional lateral load: Experimental and numerical investigation. Thin-Walled Struct 2017;119:178–89. http://dx.doi.org/10.1016/j.tws.2017.06.002.

[71] Jiao P, Chen Z, Ma H, Ge P, Gu Y, Miao H. Buckling behaviors of thin-walled cylindrical shells under localized axial compression loads, Part 1: experimental study. Thin-Walled Struct 2021;166:108118. http://dx.doi.org/10.1016/j.tws.2021.108118.

[72] Baciu TD, Degenhardt R, Franzoni F, Gliszczynski A, Arbelo MA, Castro SGP, et al. Sensitivity analysis for buckling characterisation using the vibration correlation technique. Thin-Walled Struct 2023;183:110329. http://dx.doi.org/10.1016/j.tws.2022.110329.